Sr2Ir1-xCuxO4 (x = 0, 0.05 and 0.1): Dilute magnetism in a mixed 3d–5d transition-metal oxide

Sourav Marik, Loryne Lefevre, Sébastien Fourcade, Rodolphe Decourt, Olivier Toulemonde

▶ **To cite this version:**

Sourav Marik, Loryne Lefevre, Sébastien Fourcade, Rodolphe Decourt, Olivier Toulemonde. Sr2Ir1-xCuxO4 (x = 0, 0.05 and 0.1): Dilute magnetism in a mixed 3d–5d transition-metal oxide. Journal of Alloys and Compounds, 2018, 735, pp.1908-1913. 10.1016/j.jallcom.2017.11.283 . hal-01671437

HAL Id: hal-01671437
https://hal.science/hal-01671437

Submitted on 8 Nov 2023

HAL is a multi-disciplinary open access archive for the deposit and dissemination of scientific research documents, whether they are published or not. The documents may come from teaching and research institutions in France or abroad, or from public or private research centers.

L'archive ouverte pluridisciplinaire **HAL**, est destinée au dépôt et à la diffusion de documents scientifiques de niveau recherche, publiés ou non, émanant des établissements d'enseignement et de recherche français ou étrangers, des laboratoires publics ou privés.

$Sr_2Ir_{1-x}Cu_xO_4$ (x = 0, 0.05 and 0.1): Dilute magnetism in a mixed *3d – 5d* transition-metal oxide

Marik S. [a], Lefevre L. [a], Fourcade S. [a], Decourt R. [a], Toulemonde O. [a]

[a] *CNRS, Université de Bordeaux, ICMCB, 87 Avenue du Dr. A. Schweitzer, Pessac, F-33608, France*

Abstract :

Herein we have investigated the effect of Cu (*3d* − transition metal) substitution for the Ir – site on the structure and physical properties of Sr_2IrO_4. Interestingly, the critical octahedral rotation is found to decrease (increase in Ir – O – Ir angle) with Cu substitution. The resistivity measurements illustrate a significant decrease with Cu substitution, however, keep a semiconducting dependence. Magnetic measurements reveal a decrease in the magnetic transition temperatures. Observed magnetic moment per metal ion shows a decreasing trend as Cu content is increased in the structure. A study of the composition – structure – properties correlation for this interesting and mixed *3d* − *5d* transition metal system is presented and discussed here.

1. Introduction

Over the past few decades, transition metal oxides (TMOs) have attracted immense attention in solid state physics and chemistry due to the rich and intriguing physicochemical behaviors, such as high-Tc superconductivity in cuprates [1], colossal magnetoresistance in manganates [2], and multiferroicity in Bismuth compounds [3]. Recently, iridium (Ir) based *5d* transition metal oxides have sparked significant interest due to the potential to host exotic physicochemical properties driven by the strong spin − orbit coupling (SOC) [4–19]. Due to the large atomic mass and extended nature of the *5d* orbital, *5d* − iridates tend to display strong relativistic SOC and crystal field effect (CEF); these, in fact, offset the relative weakness of the Coulomb interaction. Subsequently, in terms of physical properties, *5d* − iridates are usually dramatically different from their 3d counterparts.

The perovskite-based layered compound Sr_2IrO_4 with a celebrated K_2NiF_4 structure has attracted particular interest among the *5d* − iridate oxide materials [16,20]. Sr_2IrO_4 crystallizes in a tetragonal structure with $I4_1/acd$ space group. As mentioned earlier, this structure is a form of K_2NiF_4 structure shared by La_2CuO_4 and Sr_2RuO_4, differing by ~11° rotation of the IrO_6 octahedra around [001] direction [20]. This rotation of the octahedra lowers the symmetry space group (S.G.) of Sr_2IrO_4 from $I4/mmm$ to $I4_1/acd$. Concerning the electronic structure, Sr_2IrO_4 is revealed to host a $J_{eff} = 1/2$ Mott spin-orbit insulating state and accordingly, it exhibits antiferromagnetic (AFM) ordering at 240 K with canted magnetic moments [21–23]. The saturation magnetic moment is $0.14\mu_B$/Ir along the [100] direction, and the net ferromagnetic moments are stacked along the [001] direction with an up – down – down – up AFM configuration. The similarity of the magnetic insulating state and the crystal structure with the layered cuprate (La_2CuO_4) has steered the interest in realizing superconductivity via doping [19,24–26].

Several studies in the form of the electron, hole, and iso-−electronic doping have been experimentally performed to date and showed the intriguing evolution of physical properties with doping. Cao et al. [27] found that insulator to metal (I-M) transition and an exotic metallic state induced by very dilute electron − doping (with dilute oxygen vacancies) in Sr_2IrO_4. Recently, Kim et al. [19] using photoemission experiments showed the formation of d − wave gap at low temperatures with 6–8% electron doping on the surface of Sr_2IrO_4. A new long-range magnetic structure emerged upon 10% Mn doping (for the Ir − site) through a reordering of the spins from the basal plane to the [001] direction [28]. Rh substitution (for the Ir − site) on the Sr_2IrO_4 phase has revealed a rich phase diagram with multiple electronic and magnetic transitions [29,30]. Instead of isoelectronic Rh^{4+} ($4d^5$) substitution as expected in a first assumption, Rh-doping introduces Rh^{3+}/Ir^{5+}

* Corresponding author.
E-mail address: soumarik@gmail.com (S. Marik).

ions, and a novel spin-orbit percolation theory is suggested to understand the magnetic phase diagram of these materials.

Despite the aforesaid efforts, the study on the evolution of physical properties with doping (electron and hole) for this interesting phase is still at the initial stage. There is still much to learn about the impact of doping on the spin − orbital Mott − insulating ground state, and it is yet to explore how robust the gapped $J_{eff} = 1/2$ state is to perturbations (such as doping), which can then act as a vehicle to trigger novel phases. Furthermore, in earlier studies, substitutions for the Ir − site was focused mainly on the isovalent cations (Ti^{4+}, Mn^{4+}, Fe^{4+}, Co^{4+}, Ru^{4+}, only Rh substitution introduces Rh^{3+}, instead of isovalent/isoelectronic Rh^{4+}) [20,28–32]. Therefore, the impact of non − isovalent substitution for the Ir − site on the SOC of the Sr_2IrO_4 is of interest. In this paper, we present and discuss the impact of Cu (*3d* − cation, Cu^{2+}, Cu^{3+}) doping on the structure and physical properties of the Sr_2IrO_4 system.

2. Experimental section

Polycrystalline samples of nominal compositions $Sr_2Ir_{1-x}Cu_xO_4$ (x = 0, 0.05 and 0.1) were prepared by standard solid state reaction method, starting from stoichiometric amount of $SrCO_3$ (99.9%), CuO (99.99%) and Ir metal powder (99.99%). Starting materials were repeatedly ground and heat treated several times before final sintering of pellet at 1373 K for 24 h in the air, this step was repeated twice.

All the samples were characterized by X-ray powder diffraction (XRD) at room temperature (RT), performed in a Philips X'Celerator diffractometer (Cu $K_{\alpha 1}$-radiation, λ = 1.5406 Å). The XRD patterns were refined with the Rietveld procedure.

Oxygen contents of all the samples were determined in a thermogravimetric analysis (TGA) system. The thermal analysis was carried out in a reducing atmosphere (95% Ar + 5% H_2) over a temperature range of RT − 973 K with a heating/cooling rate of 1.5 K/min. Samples were heated to 973 K then isothermally maintained for 6 h, and cooled down to room temperature. The oxygen contents were calculated considering that the final products were SrO, Ir, and Cu as observed by the X-ray diffraction.

Temperature dependent direct current (dc) magnetic measurements were performed over the temperature range 5–300 K, using a Squid Quantum Design XL-MPMS magnetometer. DC magnetic measurements were performed in zero field cooling (ZFC) and field cooling (FC) conditions. Resistivity and Specific heat measurements were performed using a Quantum Design PPMS.

3. Results and discussion

3.1. Structure and oxygen content

Rietveld refinement of RT − XRD patterns (Fig. 1a) indicates that all the compounds (x = 0, 0.05 and 0.1) can be isolated as a single phase, crystallizing in a tetragonal symmetry with $I4_1/acd$ space group, isostructural with the parent (Sr_2IrO_4, x = 0) compound. The obtained lattice parameters and the agreement factors resulting from the refinements of RT − XRD data are given in Table 1. Ir − O bond lengths (d, in Å) and bond angle (°) are given in Table 2. The crystal structure is shown in Fig. 1b. The oxygen contents as obtained from the TGA measurements (Figure S1 in the Supporting Information) are ~ 4 for Sr_2IrO_4 and $Sr_2Ir_{0.9}Cu_{0.1}O_4$, indicating no oxygen stoichiometry deviation as often observed for *3d* transition metal oxides with K_2NiF_4 − type structure (for instance in $La_2TMO_{4\pm\delta}$ materials, *TM* = Co [33], Ni [34], Cu [35]).

Fig. 2a shows the variation of the lattice parameters (a and c) with substituted Cu content in the structure. Interestingly, substitution of Cu for the Ir-site results in a nearly uniform increment in the a axis and shortening along c. However, the unit cell volume (V)

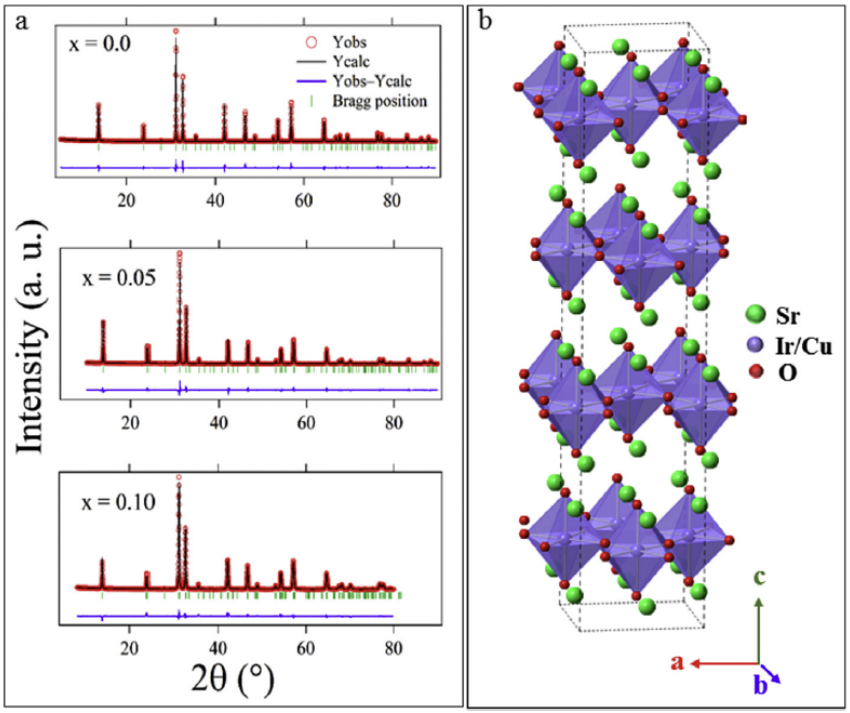

Fig. 1. (a) Final observed, calculated and difference profiles (Tetragonal, $I4_1/acd$) of the RT − XRD patterns for $Sr_2Ir_{1-x}Cu_xO_4$ samples (x = 0, 0.05 and 0.1). (b) The crystal structure of the $Sr_2Ir_{1-x}Cu_xO_4$ samples at room temperature.

Table 1
Refined crystallographic parameters and reliability factors obtained from Rietveld refinement of the RT – XRD patterns for the $Sr_2Ir_{1-x}Cu_xO_4$ samples.

	x = 0	x = 0.05	x = 0.1
a (Å) = b (Å)	5.4959 (1)	5.5029 (1)	5.5083 (1)
c (Å)	25.7893 (4)	25.7089 (3)	25.6223 (4)
V (Cell Volume, Å^3)	778.97 (2)	778.52 (1)	777.43 (2)
Sr (0, 0, z)			
z	0.5504 (1)	0.5504 (1)	0.5505 (1)
B_{iso}	1.7 (1)	2.2 (1)	2.1 (1)
Ir/Cu (0, 0.25, 0.375)			
Occupancy	1.00/0.00	0.96 (1)/0.04 (1)	0.88 (2)/0.12 (2)
B_{iso}	1.03 (5)	1.6 (1)	0.5 (2)
O1 (0, 0.25, z)			
z	0.4565 (4)	0.4544 (2)	0.4621 (1)
O2 (x, y, 0.125)			
x	0.297 (1)	0.290 (1)	0.287 (1)
y	0.547 (1)	0.540 (1)	0.537 (1)
R_P	9.78	9.34	7.80
R_{Bragg}	2.70	2.67	3.37
χ^2	7.99	4.19	2.14

Table 2
Ir–O bond lengths (d, in Å) and bond angles in deg for the $Sr_2Ir_{1-x}Cu_xO_4$ samples at RT. O1 refers to the apical oxygen, O2 refers to the basal oxygen.

	x = 0	x = 0.05	x = 0.1
d_{Ir-O1} (Å)	2.09 (1)	2.07 (1)	2.21 (1)
d_{Ir-O2} (Å)	1.978 (1)	1.97 (1)	1.969 (1)
Ir – O1 – Ir (°)	180	180	180
Ir – O2 – Ir (°)	158.4 (1)	161.9 (1)	163.1 (1)

is found to decrease with increasing Cu content in the structure (Figure S2 in the Supporting Information). This behavior can be understood if we consider that the most of the substituted Cu is in 3+ oxidation state since the ionic radius of Cu^{3+} (low spin, 0.54 Å) is smaller than Ir^{4+} (0.625 Å) [An increase in the unit cell volume would be expected instead for Cu^{2+} doping because of its larger ionic radius (0.73 Å)]. The Cu^{3+} (and/or small quantity of Cu^{2+}) in the structure introduces Ir^{5+} to preserve the charge neutrality (oxygen content is almost same for all the studied sample, see figure S1 in the SI). The increment in the a axis with Cu doping could be due to the reduction of the octahedral rotation (Fig. 2b). A similar phenomenon is observed also for the La – doped [36] (for the Sr – site) and Sr vacant [37] Sr_2IrO_4 samples.

3.2. Resistivity

Fig. 3 shows the temperature variation of resistivity for all the samples. Similarly to the earlier studies, the resistivity of the parent compound (Sr_2IrO_4) is insulating [38,39]. Interestingly, a remarkable decrease in the resistivity (decreased by a factor of 10^4 at 80 K) is observed with Cu doping, and both the Cu-doped samples (x = 0.05 & 0.1) show semiconducting behavior down to 5 K. It is noteworthy that the octahedral rotation, which is indeed critical to electron hopping between active t_{2g} orbitals, is decreasing with Cu substitution.

To understand the mechanism of conduction at low temperature (5 K–40 K), the resistivity data for x = 0.05 and 0.1 samples are analyzed by fitting to Arrhenius – type behavior and Mott variable range hopping (VRH) type behavior expected for a three-dimensional (3D) disordered system (Fig. 4). These two models can be expressed as $\rho(T) = \rho_0 \exp(T_0/T)^{1/(d+1)}$, for the Arrhenius model d = 0, T_0 is the activation energy for a semiconductor and for the 3D – VRH model d = 3 and T_0 is the characteristic energy for hopping. The Arrhenius model does not follow a straight line in the low-temperature region; however, the fitting with the 3D – VRH model shows a straight–line behavior. The characteristic energy for hopping is found to increase ($T_0 = 1.2\,(1) \times 10^4$ K and $1.9\,(1) \times 10^4$ K for x = 0.05 and 0.1, respectively) with increasing Cu content in the structure. This is attributed to the enhancement in the density of electronic states at Fermi level as observed in the specific heat measurements (discussed in paragraph 3.4). For the polycrystalline Sr_2IrO_4 a 3D – VRH model was suggested in the low-temperature region (35–80 K) [38]. Recently, Bhatti et al. [39] highlighted a 2D – Mott VRH model in the low-temperature region (5–40 K) for the parent Sr_2IrO_4 compound. Interestingly, for the present Cu-doped samples, the 3D – VRH model gives better approximation (2D – VRH model is shown in figure S3 of the SI) of the data than the 2D – VRH. The 3D – VRH type behavior for x = 0.05 and 0.1 samples could be due to the enhanced chemical disorder introduced by the Cu (Cu is randomly distributed) substitution.

3.3. Magnetism

Fig. 5 shows the temperature variation of magnetic susceptibility (χ–T) for all the studied samples measured in an applied magnetic field of 1000 Oe (0.1 T). For the parent Sr_2IrO_4 compound, the χ – T data are in accordance with previous results; a sharp

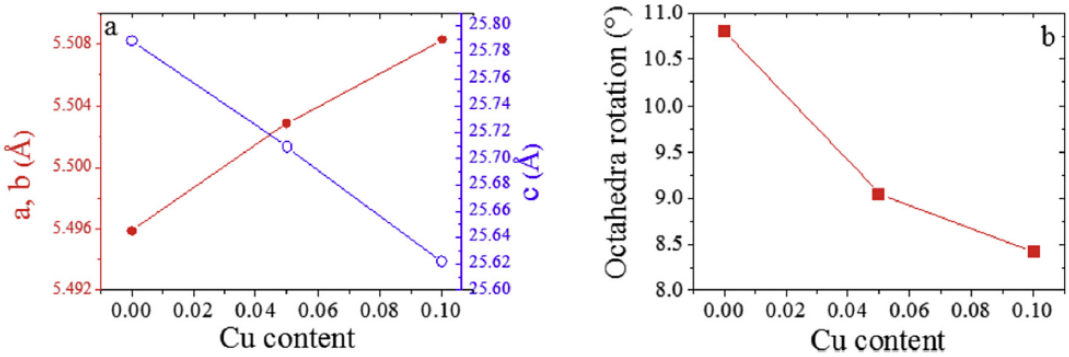

Fig. 2. Variation of (a) lattice parameters (a, b and c) and (b) octahedra rotation with doped Cu concentration for $Sr_2Ir_{1-x}Cu_xO_4$ samples as obtained from the RT – XRD Rietveld refinements. At RT, the nearly uniform increment in the a axis and shortening along c is observed with increasing Cu doping concentration in the structure. Concurrently, octahedra rotation (increase in Ir – O – Ir bond angle) is decreasing with increasing Cu content in the structure.

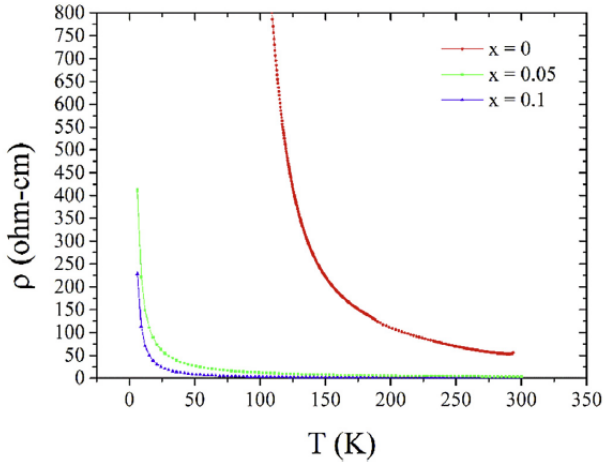

Fig. 3. Temperature variation of the resistivity for $Sr_2Ir_{1-x}Cu_xO_4$ samples. A significant decrease in the resistivity (decreased by a factor of 10^4 at 80 K) is observed with Cu doping, however, both the Cu-doped samples (x = 0.05 and 0.1) show semiconducting behavior down to 5 K.

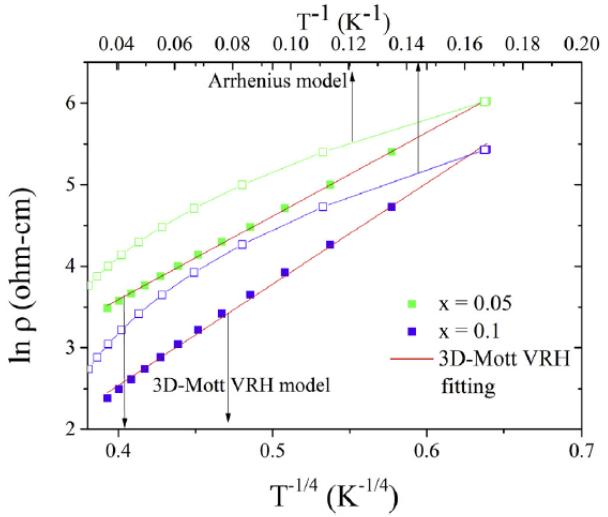

Fig. 4. The temperature dependent resistivity for $Sr_2Ir_{0.95}Cu_{0.05}O_4$ (x = 0.05) and $Sr_2Ir_{0.9}Cu_{0.1}O_4$ (x = 0.1) from 5 to 40 K plotted according to the Arrhenius and 3D − Mott variable range hopping (3D − VRH) behaviors (the top and bottom axes, respectively).

magnetic transition below $T_C \approx 240$ K due to the Dzyaloshinskii − Moriya (DM) interaction [22,23]. Interestingly, with Cu substitution, the magnetic transition temperature and the magnitude of the magnetization are decreased. The effective paramagnetic moments (μ_{eff}), estimated from the modified Curie − Weiss law $\chi = \chi_0 + \mu_{eff}^2/3k_B(T - \theta)$, [$\chi_0$ is the temperature independent paramagnetism, k_B = Boltzmann constant, and θ is the Weiss temperature, shown in the inset of Fig. 5] in the temperature range of 250–300 K, unambiguously show a decreasing trend with increasing Cu content in the structure (Fig. 6). At the same time, χ_0 follows an increasing direction with Cu substitution; this could be attributed to the VanVleck − type paramagnetic contribution due to the introduction of the nonmagnetic $5d^4$ − Ir^{5+} cations in the structure with respect to the diamagnetic contribution given by the core electrons [40]. The estimated μ_{eff} and χ_0 for the parent Sr_2IrO_4 compound are

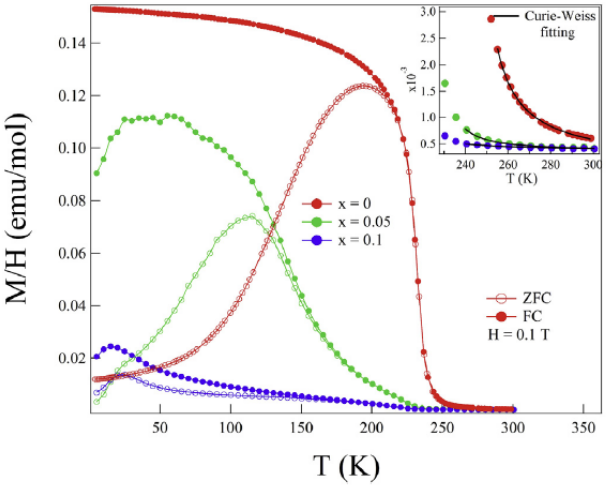

Fig. 5. Temperature dependence FC and ZFC susceptibility curves in an external field of 0.1 T for $Sr_2Ir_{1-x}Cu_xO_4$ (x = 0, 0.05 & 0.1) samples. The inset shows the Curie-Weiss fitting of the FC susceptibility curves.

comparable with the previous studies [23,39,40].

To investigate the magnetic properties of the compounds further, the isothermal magnetization curves (M − H) for all the samples are measured at 5 K with a field range of ±4T and shown in Fig. 7. The measured magnetization curve for the parent Sr_2IrO_4 sample shows the nonsaturating behavior with a magnetization value of $\mu_H = 0.05\ \mu_B$/f.u. at 4 T, and consistent with earlier reports. Interestingly, with Cu substitution, the S−shaped (nonlinear) canted AFM like behavior in the M − H plot decreases continuously, and the $Sr_2Ir_{0.9}Cu_{0.1}O_4$ (x = 0.1) shows an almost linear variation with the magnetic field. However, the clear hysteresis, observed for both the Cu-doped samples (x = 0.05 and 0.1) at 5 K indicates the existence of magnetic frustration in the layered structure.

The overall magnetic behavior of the $Sr_2Ir_{1-x}Cu_xO_4$ samples can be explained by considering two key ingredients: (i) Cu substitution effect, and (ii) decrease in the octahedral rotation as a result of Cu substitution. Cu substitution actually introducing pairs of nonmagnetic cations [Cu^{3+} (low spin) and Ir^{5+}], and indeed makes the magnetic interactions diluted. A similar situation arises with Rh^{3+} doping, and a novel spin − orbital percolation picture was

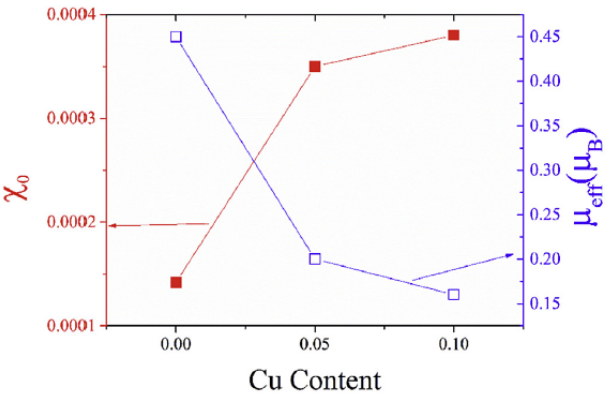

Fig. 6. Variation of temperature independent susceptibility contributions (χ_0, left axis), and effective paramagnetic moments (μ_{eff}, right axis) with doped Cu concentration for $Sr_2Ir_{1-x}Cu_xO_4$ (x = 0, 0.05 & 0.1) samples.

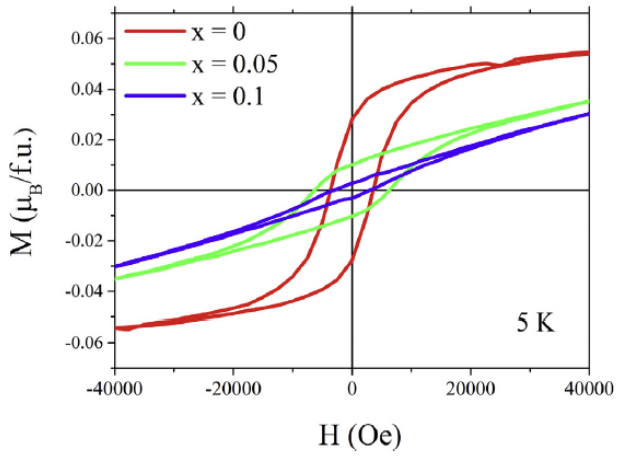

Fig. 7. Isothermal magnetization (M − H) curves for $Sr_2Ir_{1-x}Cu_xO_4$ samples collected at T = 5 K.

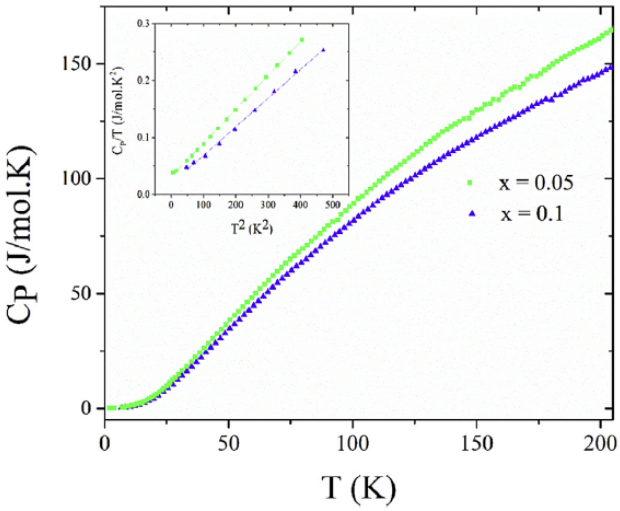

Fig. 8. Temperature variation of specific heat (C_P − T) for $Sr_2Ir_{0.95}Cu_{0.05}O_4$ (x = 0.05) and $Sr_2Ir_{0.9}Cu_{0.1}O_4$ (x = 0.1). The inset shows the specific heat plotted as C_P/T *vs.* T^2 for 4 < T < 22.5 K.

suggested to explain the dilute magnetism in that system [30]. In that scenario, Rh doping level of x = 0.21 was sufficient to exceed the percolation threshold and showed the complete disappearance of magnetic order. Nevertheless, for the present case the possibility of the presence of magnetic Cu^{2+} (in addition to the magnetic Ir^{4+}) cations, even in a little amount, may originate complex magnetic interactions. In fact, the peak at 25 K, observed in the susceptibility data for the x = 0.1 sample (Fig. 5) could be a result of the magnetic frustration associated with the presence of several magnetic cations (Cu^{2+} and Ir^{4+}) diluted in a nonmagnetic matrix of Cu^{3+} (low spin) and Ir^{5+}. This could originate finite size clusters with short-range magnetic correlations. Indeed, the clear hysteresis with enhanced linear behavior observed in the M − H plot for the Cu substituted samples indicates the existence of magnetic frustration. On the other hand, a remarkable correlation between cooperative octahedral rotations and Ir magnetic moments deviating away from the a axis and then leading to a net moment projected along b axis was proposed earlier [23]. Thus, in addition to the impact of the dilution of the Ir^{4+} paramagnetic cations, the decrease in the octahedral rotation with Cu substitution could also suppress the magnetism by reducing the canting of the Ir^{4+} magnetic moments.

3.4. Specific heat

In the specific heat for Cu substituted samples, there is, however, no indication for a magnetic transition down to 2 K. It is noteworthy that no anomaly was observed in specific heat data for the parent sample (Sr_2IrO_4). The specific heat at low temperatures (inset in Fig. 8) is well described by C_P (T) = γT + βT^3. The coefficient for electronic contribution, γ, systematically increases with x (Cu substitution) from 18 (2) mJ K^{-2} mol^{-1} (for x = 0.05, for the parent Sr_2IrO_4 compound γ = 2 mJ K^{-2} mol^{-1} [38,39]) to 30 (2) mJ K^{-2} mol^{-1} at x = 0.1. The increment in the γ value is due to the enhancement in the density of electronic states at Fermi level suggesting a hole − doping effect with Cu substitution.

4. Conclusions

In summary, the structural, magnetic, transport and thermal properties of not isovalent Cu substitution for the Ir − site on the SOC of Sr_2IrO_4 are explored. From the structural point of view, Cu substitution into the spin − orbit Mott insulator $Sr_2Ir_{1-x}Cu_xO_4$ diminishes the Ir^{4+} content in samples; this assist to reduce the unit cell c−axis due to the cancellation of the Jahn − Teller distortion of the IrO_6 octahedra.

The resistivity measurements illustrate a significant decrease with Cu substitution, however, keep a semiconducting dependence. A 3D − VRH model is suggested to explain the electronic conduction mechanism at low temperature for the Cu substituted samples (x = 0.05 and 0.1).

Magnetic measurements reveal a decrease in the magnetic transition temperatures and observed magnetic moment per metal ion as Cu content is increased in the structure. Along with the linear like M − H behavior, the clear hysteresis, observed for the Cu-doped samples at 5 K indicates the existence of magnetic frustration. Cu doping actually introduces nonmagnetic Cu^{3+} and Ir^{5+} cations in the structure; this leads to the magnetic dilution of the system. Since Cu doping effectively hole − dope the system, a systematic increment in the γ value with Cu substitution is observed due to the enhancement in the density of electronic states at Fermi level.

Considering the capability of the materials containing both *3d* and *5d* magnetic cations to host new physics absent in either pure *3d* or pure *5d* compounds; this interesting mixed *3d* − *5d* $Sr_2Ir_{1-x}Cu_xO_4$ system is clearly inviting further in−depth physicochemical investigations (such as thermoelectric power, Hall, photoemission spectroscopy studies) in order to elucidate the physical mechanisms at work in this system.

Acknowledgements

The authors are indebted to the CNRS and Université Bordeaux for funding this work. SM acknowledges 'Chimie exploratoire' thematic (ICMCB) for his postdoctoral financial support.

Appendix A. Supplementary data

Supplementary data related to this article can be found at https://doi.org/10.1016/j.jallcom.2017.11.283.

References

[1] J.G. Bednorz, K.A. Müller, M. Takashige, Science 236 (1987) 73−75.
[2] R. von Helmolt, J. Wecker, B. Holzapfel, L. Schultz, K. Samwer, Phys. Rev. Lett. 71 (1993) 2331.

[3] T. Zhao, A. Scholl, F. Zavaliche, K. Lee, M. Barry, A. Doran, M.P. Cruz, Y.H. Chu, C. Ederer, N.A. Spaldin, R.R. Das, D.M. Kim, S.H. Baek, C.B. Eom, R. Ramesh, Nat. Mater. 5 (2006) 823–829.
[4] B.J. Kim, Hosub Jin, S.J. Moon, J.-Y. Kim, B.-G. Park, C.S. Leem, Jaejun Yu, T.W. Noh, C. Kim, S.-J. Oh, J.-H. Park, V. Durairaj, G. Cao, E. Rotenberg, Phys. Rev. Lett. 101 (2008) 076402.
[5] B.J. Kim, H. Ohsumi, T. Komesu, S. Sakai, T. Morita, H. Takagi, T. Arima, Science 323 (2009) 1329.
[6] W. Witczak-Krempa, G. Chen, Y.B. Kim, K. Balents, Annu. Rev. Condens. Matter Phys. 5 (2014) 57.
[7] S. Nakatsuji, Y. Machida, Y. Maeno, T. Tayama, T. Sakakibara, J. van Duijn, L. Balicas, J.N. Millican, R.T. Macaluso, J.Y. Chan, Phys. Rev. Lett. 96 (2006) 087204.
[8] M.C. Shapiro, S.C. Riggs, M.B. Stone, C.R. de la Cruz, S. Chi, A.A. Podlesnyak, I.R. Fisher, Phys. Rev. B 85 (2012), 214434.
[9] Y. Singh, S. Manni, J. Reuther, T. Berlijn, R. Thomale, W. Ku, S. Trebst, P. Gegenwart Phys, Rev. Lett. 108 (2012), 127203.
[10] Y. Okamoto, M. Nohara, H. Aruga-Katori, H. Takagi, Phys. Rev. Lett. 99 (2007), 137207.
[11] S.J. Moon, H. Jin, K.W. Kim, W.S. Choi, Y.S. Lee, J. Yu, G. Cao, A. Sumi, H. Funakubo, C. Bernhard, T.W. Noh, Phys. Rev. Lett. 101 (2008) 226402.
[12] G. Jackeli, G. Khaliullin, Phys. Rev. Lett. 102 (2009) 017205.
[13] W. Fa, T. Senthil, Phys. Rev. Lett. 106 (2011) 136402.
[14] Y. Yang, W.-S. Wang, J.-G. Liu, H. Chen, J.-H. Dai, Q.-H. Wang, Phys. Rev. B 89 (2014), 094518.
[15] S. Bahr, A. Alfonsov, G. Jackeli, G. Khaliullin, A. Matsumoto, T. Takayama, H. Takagi, B. Büchner, V. Kataev, Phys. Rev. B 89 (2014), 180401.
[16] M.K. Crawford, M.A. Subramanian, R.L. Harlow, J.A. Fernandez-Baca, Z.R. Wang, D.C. Johnston, Phys. Rev. B 49 (1994) 9198.
[17] Y. Cao, Q. Wang, J.A. Waugh, T.J. Reber, H. Li, X. Zhou, S. Parham, S.-R. Park, N.C. Plumb, E. Rotenberg, A. Bostwick, J.D. Denlinger, T. Qi, M.A. Hermele, G. Cao, D.S. Dessau, Nat. Commun. 7 (2016) 11367.
[18] M.P.M. Dean, Y. Cao, X. Liu, S. Wall, D. Zhu, R. Mankowsky, V. Thampy, X.M. Chen, J.G. Vale, D. Casa, Jungho Kim, A.H. Said, P. Juhas, R. Alonso-Mori, J.M. Glownia, A. Robert, J. Robinson, M. Sikorski, S. Song, M. Kozina, H. Lemke, L. Patthey, S. Owada, T. Katayama, M. Yabashi, Y. Tanaka, T. Togashi, J. Liu, C. Rayan Serrao, B.J. Kim, L. Huber, C.-L. Chang, D.F. McMorrow, M. Först, J.P. Hill, Nat. Mater. 15 (2016) 601–605.
[19] Y.K. Kim, N.H. Sung, J.D. Denlinger, B.J. Kim, Nat. Phys. 12 (2016) 37–41.
[20] Q. Huang, J.L. Soubeyroux, O. Chmaissen, I. Natali Sora, A. Santoro, R.J. Cava, J.J. Krajewski, W.F. Peck Jr., J. Solid State Chem. 112 (1994) 355.
[21] S.J. Moon, M.W. Kim, K.W. Kim, Y.S. Lee, J.-Y. Kim, J.-H. Park, B.J. Kim, S.-J. Oh, S. Nakatsuji, Y. Maeno, I. Nagai, S.I. Ikeda, G. Cao, T.W. Noh, Phys. Rev. B 74 (2006) 113104.
[22] G. Cao, J. Bolivar, S. McCall, J.E. Crow, R.P. Guertin, Phys. Rev. B 57 (1998). R11039(R).
[23] F. Ye, S. Chi, B.C. Chakoumakos, J.A. Fernandez-Baca, T. Qi, G. Cao, Phys. Rev. B 87 (2013) 140406.
[24] H. Watanabe, T. Shirakawa, S. YunokiPhys, Rev. Lett. 110 (2013), 027002.
[25] Y. Yang, W.-S. Wang, J.-G. Liu, H. Chen, J.-H. Dai, Q.-H. Wang, Phys. Rev. B 89 (2014), 094518.
[26] Y. Gao, T. Zhou, H. Huang, Q.-H. Wang, Sci. Rep. 5 (2015) 9251.
[27] O.B. Korneta, T. Qi, S. Chikara, S. Parkin, L.E. De Long, P. Schlottmann, G. Cao, Phys. Rev. B 82 (2010), 115117.
[28] F. Ye, S. Chi, Bryan C. Chakoumakos, Jaime A. Fernandez-Baca, T. Qi, G. Cao, Phys. Rev. B 87 (2013), 140406(R).
[29] T.F. Qi, O.B. Korneta, L. Li, K. Butrouna, V.S. Cao, X. Wan, P. Schlottmann, R.K. Kaul, G. Cao, Phys. Rev. B 86 (2012), 125105.
[30] J.P. Clancy, A. Lupascu, H. Gretarsson, Z. Islam, Y.F. Hu, D. Casa, C.S. Nelson, S.C. LaMarra, G. Cao, Y.-J. Kim, Phys. Rev. B 89 (2014) 054409.
[31] M. Ge, S. Tan, J. Shao, L. Pi, Y. Zhang, J. Magn. Magn Mater. 369 (2014) 223–227.
[32] A.J. Gatimu, R. Berthelot, S. Muir, A.W. Sleight, M.A. Subramanian, J. Solid State Chem. 190 (2012) 257–263.
[33] R.A. Mohan Ram, P. Ganguly, C.N.R. Rao, J.M. Honig, Mater. Res. Bull. 23 (1988) 501–506.
[34] A. Demourgues, P. Dordor, J.-P. Doumerc, J.-C. Grenier, E. Marquestaut, M. Pouchard, A. Villesuzanne, A. Wattiaux, J. Solid State Chem. 124 (1996) 199–204.
[35] T. Hirayama, M. Nakagawa, A. Sumiyama, Y. Oda, Phys. Rev. B 58 (1998) 5856.
[36] C. Cosio-Castaneda, G. Tavizon, A. Baeza, P. de la Mora, R. Escudero, J. Phys. Condens. Matter 19 (2007) 446210.
[37] X. Suna, S.L. Liub, H. Wangb, B. Lib, J. Chengb, Z.H. Wang, J. Alloy. Comp. 687 (2016) 712–719.
[38] N.S. Kini, A.M. Strydom, H.S. Jeevan, C. Geibel, S. Ramakrishnan, J. Phys. Condens. Matter 18 (2006) 8205.
[39] I.N. Bhatti, R. Rawat, A. Banerjee, A.K. Pramanik, J. Phys. Condens. Matter 27 (2014), 016005.
[40] T. Dey, A. Maljuk, D.V. Efremov, O. Kataeva, S. Gass, C.G.F. Blum, F. Steckel, D. Gruner, T. Ritschel, A.U.B. Wolter, J. Geck, C. Hess, K. Koepernik, J. van den Brink, S. Wurmehl, B. Buchner, Phys. Rev. B 93 (2016) 014434.